MST kinases monitor actin cytoskeletal integrity and signal via JNK stress-activated kinase to regulate p21$^{Waf1/Cip1}$ stability.

Running title: MST regulation by cytoskeletal integrity

Ruth Densham[†], Eric O'Neill[*], June Munro, Ireen König, Kurt Anderson, Walter Kolch, Michael F. Olson[*]

The Beatson Institute for Cancer Research, Garscube Estate, Switchback Road, Glasgow UK G61 1BD

[*]Corresponding Author:
Michael F Olson
The Beatson Institute for Cancer Research, Garscube Estate, Switchback Road, Glasgow UK G61 1BD
Tel: +44 (0)141 330 3654
m.olson@beatson.gla.ac.uk

Word count for Materials and Methods: 1,345

Word count for Introduction, Results, Discussion: 3,545

[†]Present Address: Cancer Genetics Laboratory, Dept Medical & Molecular Genetics, King's College Medical School, Guy's Hospital, Tower Wing, Great Maze Pond, London, SE1 9RT

[*]Present Address: Radiation Oncology and Biology, University of Oxford, Old Road Campus Research Building, Churchill Hospital, Oxford OX3 7DQ

ABSTRACT

As well as providing a structural framework, the actin cytoskeleton also plays integral roles in cell death, survival and proliferation. Disruption of the actin cytoskeleton results in activation of the JNK stress-activated protein kinase (SAPK) pathway, however, the “sensor” of actin integrity that couples to the JNK pathway has not been characterized in mammalian cells. We now report that the MST kinases mediate the activation of the JNK pathway in response to disruption of the actin cytoskeleton. One consequence of actin disruption is the JNK-mediated stabilization of $p21^{Waf1/Cip1}$ (p21) via phosphorylation on Thr57. Expression of MST1 or MST2 was sufficient to stabilize p21 in a JNK- and Thr57-dependent manner, while the stabilization of p21 by actin disruption required MST-activity. These data indicate that, in addition to being components of the Salvador-Warts-Hippo tumour suppressor network and binding partners of c-Raf and the RASSF1A tumour suppressor, MST kinases serve to monitor cytoskeletal integrity and couple via the JNK SAPK pathway to the regulation of a key cell cycle regulatory protein.

INTRODUCTION

The actin cytoskeleton is a dynamic structure that determines cell morphology and motility. In addition, the cytoskeleton also influences other biological functions such as proliferation, survival and death, although the mechanistic details linking the cytoskeleton to these processes have not been fully elucidated. Considerable effort has focused on characterizing the signal transduction pathways that control cytoskeletal organization (33). The actin cytoskeleton itself may also regulate cell signalling; for example, mechanical stretching, shear stress and cytoskeletal disruption have each been shown to activate stress-activated protein kinase (SAPK) pathways (34). Although in *Saccharomyces cerevisiae* an actin-integrity responsive pathway has been identified in which actin cytoskeleton disassembly results in activation of the Ssk2p kinase that lies upstream of the Hog1 SAPK pathway (7, 56), an analogous pathway in mammalian cells has not been delineated.

SAPK pathways are specific examples of mitogen-activated protein kinase (MAPK) cascades (43). At the bottom of archetypal MAPK pathways are signal propagating kinases such as ERK1 and ERK2; in the case of SAPK signalling the similarly positioned kinases are JNK and p38 family members. MAPK are phosphorylated and regulated by MAPK kinases (MAP2K); for JNK the MAP2K are MKK4 and MKK7 while for p38 they are MKK3 and MKK6. Moving stepwise further upstream are MAP3K and MAP4K, although in some pathways there may be no need for a MAP4K, Ras activation of the MAP3K Raf in the ERK MAPK pathway being one example.

Although much recent interest has focused on their anti-proliferative and pro-apoptotic functions as a component of the Salvador-Warts-Hippo

tumour suppressor network (31) and as binding partners of the c-Raf MAP3K (40) and RASSF1A tumour suppressor (39), the Mammalian Ste20-like (MST) kinases 1 and 2 were first identified (17) because of their homology with the *Saccharomyces cerevisiae* Ste20 MAP4K that acts as upstream of three MAPK cascades, including the Ste11/Pbs2/Hog1 SAPK pathway (51). Although the MST kinase domains are very similar to those in Ste20 and mammalian p21-activated kinases (PAK), there is little homology outside this domain, as a result MST1 and MST2 make up their own Ste20 subfamily without direct orthologues prior to the emergence of the bilaterian sub-regnum. Given the homology with Ste20, initial characterization focused on the possibility that MST kinases were involved in MAPK regulation, and indeed MST kinases were found to activate SAPK pathways (27), which was associated with activation of MKK6 and MKK7 (27). It was also found that MST1 co-expression with a kinase-dead version of the MAP3K MEKK1 blocked JNK activation (26). Consistent with these results, MST1 could not activate JNK in cells deleted for both MAP2K enzymes MKK4 and MKK7 (53). Therefore, it would appear that MST kinases work at the same level (MAP4K) as Ste20 in the regulation of the SAPK pathways. Although pro-apoptotic signalling has been shown to contribute to MST activation via caspase-mediated proteolysis, which removes an autoinhibitory domain (27), there is little known about how other non-apoptotic stimuli might regulate MST.

There are several possible consequences resulting from activation of SAPK pathways in response to modifications to actin cytoskeleton organization or integrity. Actin disruption and consequent JNK activation may induce cell cycle arrest (23), apoptosis (11) or promote cell survival (2). We

previously showed that one way JNK activation following cytoskeletal disruption might contribute to cell cycle arrest is through the stabilization of the cyclin-dependent kinase inhibitor (CDKI) $p21^{Waf1/Cip1}$ (p21) (14). The eventual outcome of SAPK activation following actin cytoskeleton modification may be influenced signal intensity, duration and cellular context. Further progress towards determining how cytoskeletal disruption may generate these various outcomes will be possible when the details describing how actin cytoskeletal changes activate SAPK signalling have been established.

We wished to determine whether MST kinases might “sense” the integrity of the actin cytoskeleton and link with SAPK signalling. We found MST2 was co-localized with filamentous actin structures. Expression of MST1 or MST2 was sufficient to activate JNK1, and cytoskeletal disruption activated MST as well as JNK1 in an MST-dependent manner. One consequence of actin disruption is the JNK-mediated stabilization of p21, which was determined to be via phosphorylation on Thr57. Expression of MST1 or MST2 was sufficient to stabilize p21 in a JNK- and Thr57-dependent manner, while the stabilization of p21 by actin disruption required MST-activity. These data indicate that MST kinases serve to monitor cytoskeletal integrity and couple via the JNK SAPK pathway to the regulation of a key cell cycle regulatory protein.

MATERIALS AND METHODS

Cell culture

NIH 3T3 mouse fibroblasts and HeLa cervical carcinoma cells were grown at 5% CO_2 in Dulbecco's Modified Eagles Medium (DMEM; GibcoBRL) supplemented with penicillin and streptomycin and either 10% (v/v) donor calf serum (NIH 3T3; GibcoBRL) or fetal calf serum (HeLa; Harlan). Transient transfections were performed with Lipofectamine 2000 (Invitrogen). Cells were routinely grown in 6 cm dishes to 70% confluence. 0.5 μg plasmid DNA was incubated in 30 μl PBS + 4 μl Lipofectamine 2000 for 20 minutes before addition to 2 ml serum free DMEM and incubation on cells for 5 hours. Cells were re-stimulated with 10% donor calf serum overnight (~16 hours).

Western blots

Western blotting was performed as previously described (15). The following primary antibodies were used: Krs1/2 (MST2; C-19), RhoA (26C4), β-actin (C-4), JNK1 (C-17), p21 (C-19-G) β-tubulin (D10) from Santa Cruz; JNK1/2 (56G8), phospho c-Jun (Ser63), c-Jun, and MST1 from Cell Signalling; MST2-N-term from Epitomics; FLAG-M2 from Sigma; and ERK2 was a gift from Chris Marshall (ICR, London). Alexa-Fluor680 (Molecular Probes) or IRDye800 (Rockland)-conjugated secondary antibodies were detected and quantified by direct scanning using a Li-Cor Odyssey.

Immunofluorescence

Cells were fixed and stained for immunofluorescence as described previously (16). In brief, cells were grown on coverslips and treated as described before

fixing in 4% para-formaldehyde in PBS for 15 minutes. Coverslips were washed twice with PBS and permeablized by incubation with 0.5% Triton-X100/PBS for 10 minutes; washed three times with 1% BSA/PBS before incubation with FLAG-M2 (1:1000, Sigma) for 1 hour at room temperature; washed three times with 1% BSA/PBS before incubation with anti-mouse-FITC (1:1000) and/or Texas-Red Phalloidin (0.5 μg/ml) for 1 hour at room temperature; finally, coverslips were washed three times with 1% BSA/PBS and twice with distilled water before mounting on slides with Prolong Gold mounting media. Confocal images were obtained using an Olympus FV1000 using a 60x oil-immersion objective.

For TIRF microscopy, cells were grown in 3 cm glass-bottomed dishes (Iwaki), fixed and stained as described above. Cells were stored in PBS containing β-mercaptoethanol as an anti-fade and sealed with parafilm.

Total internal reflection microscopy

Total internal reflection fluorescence (TIRF) experiments were performed using a Nikon Eclipse TE 2000-U microscope equipped with 60x and 100x 1.45 NA Nikon TIRF oil immersion objectives. The Nikon Epifluorescence condenser was replaced with a custom condenser in which laser light was introduced into the illumination pathway directly from the optical fibre output oriented parallel to the optical axis of the microscope. The light source for evanescent wave illumination was a 473 nm diode laser or a 561 nm laser (Omicron), with each laser line coupled into the condenser separately in order to allow individual TIRF angle adjustments. The lasers were controlled by a DAC 2000 card or a Uniblitz shutter operated by MetaMorph (Molecular

Devices). A green/red dual filterblock (ET-GFP/mcherry from AHF Analysentechnik, Germany) was used for dual colour 473 nm and 561 nm excitation. A Multi-Spec dual emission splitter (Optical Insights, NM) with a 595 nm dichroic and two bandpass filters (510-565 for green and 605-655 nm for red) was used to separate both emissions. All imaging was performed with a Cascade 512F EMCCD camera (Photometrics UK).

Protein stability analysis

NIH3T3 cells were transfected as indicated and grown in serum-free media for 16 hours prior to treatment with the protein synthesis inhibitor emetine (20 μM) and combinations of Tat-C3 (0.5 μM), LTB (200 nM), CTD (200 nM) and SP600125 (30 μM) as indicated for 2 hours. Whole cell lysates were probed for p21 and ERK2, and quantified by infra-red imaging as described above.

Immunoprecipitation Assays

Cells were grown to 80% confluence in 10 cm dishes, transfected and/or treated as specified. Cells were quickly washed in ice-cold PBS, lysed in 200 μl of ice-cold TG-lysis buffer (20 mM Tris-HCl, pH8; 140 mM NaCl; 1 mM EGTA; 1% Triton X-100; 10% glycerol; 1.5 mM $MgCl_2$; 1 mM sodium vanadate; 1 mM PMSF; 20 μM leupeptin; 50 mM sodium fluoride), centrifuged (14000 x *g* for 10 minutes at 4 °C) and the protein concentration determined using the BCA protein assay kit (Pierce). Normalised lysates were immunoprecipitated by incubation with 30 μl protein A Sepharose plus antibody for Krs1/2 (MST2) or JNK1 (C-17) for 2-3 hours with rotation at 4 °C. Beads were washed three times in ice-cold buffer (50 mM Tris, pH 7.5; 200

mM NaCl; 0.1% Triton X-100) before re-suspension in Laemelli buffer and analysis by SDS-PAGE.

In-gel and immunoprecipitation kinase assays

In gel kinase assays of MST1/2 activity were performed as follows: 12% SDS-PAGE gels were poured that contained 0.5 mg/ml myelin basic protein (MBP) as a protein substrate. Samples were run as described for western blotting and then the gels were sequentially washed to remove SDS, denature and re-nature the proteins as follows: 3 x 20 minute washes in 20% propanol, 50 mM Tris pH 8; 3 x 20 minute washes in 50 mM Tris pH 8, 5 mM β-mercaptoethanol; 1x 60 minute wash in 6 M guanidine-HCl, 50 mM Tris pH 8, 5 mM β-mercaptoethanol; 3 x 20 minute washes and then overnight in 50 mM Tris pH 8, 5 mM β-mercaptoethanol, 4% Tween 20 at 4 °C; gel was re-equilibrated to room temperature in 1 x 30 minute wash 40 mM HEPES pH 8, 10 mM $MgCl_2$, 2 mM DTT; kinase assay was performed by incubation of gel with 40 mM HEPES pH 8, 10 mM $MgCl_2$, 0.5 mM EGTA, 50 μM ATP, 25 μCi γ-[^{32}P]-ATP for 2 hours at room temperature before the reaction was stopped by washing gel approx 10 times in 5% TCA, 1% sodium pyrophosphate. Finally, the gel was dried and analyzed using a phosphorimager.

For JNK immunoprecipitation/kinase assays: JNK immunoprecipitations were carried out as described above but with a final wash in SAPK buffer (20 mM HEPES pH 7.5, 20 mM β-glycerophosphate, 10 mM $MgCl_2$, 1 mM DTT, 50 μM sodium vanadate). Beads were re-suspended in 30 μl SAPK buffer containing 2.5 μg GST-cJun 1-79, 10 μM ATP and 2.5 μCi γ-[^{32}P]-ATP. Kinase reactions were carried out at 30 °C for 30 minutes with shaking and

terminated by the addition of 10 μl 4 x Laemmli sample buffer. Samples were resolved by SDS-PAGE; gels were fixed, stained with Coomassie and dried before analysis by phospho-imaging.

For recombinant JNK phosphorylation of GST-c-Jun, FLAG-p21 or FLAG-T57A: FLAG-p21 and FLAG-T57A were transiently expressed in HEK293 cells and purified by precipitation using FLAG-agarose beads (Sigma). Recombinant GST-c-Jun was expressed and purified as described (41). Beads were washed stringently 3 x with 50 mM Tris, pH 7.5; 500 mM NaCl; 0.1% Triton X-100 followed by three washes with 50 mM Tris, pH 7.5; 200 mM NaCl; 0.1% Triton X-100. JNK kinase assays were performed on the purified proteins with 0.2 μl recombinant JNK2a (Upstate/Millipore) in SAPK buffer containing 10 μM ATP and 2.5 μCi γ-[^{32}P]-ATP as described above.

Mutagenesis

Site directed mutagenesis of FLAG-p21 was carried out using the Quikchange site-directed mutagenesis kit (Stratagene) according to the manufacturer's protocol. The following PCR oligonucleotides designed to incorporate T57A, S98A, S130A, T145A, and S146A mutations were used:

T57A, forward primer 5'-CTTTGTCACCGAGGCGCCACTGGAGGGTG-3' and reverse 5'-CACCCTCCAGTGGCGCCTCGGTGACAAAG-3';

S98A, forward primer 5'-CGGCCTGGCACCGCGCCTGCTCTGCTG-3' and reverse 5'-CAGCAGAGCAGGCGCGGTGCCAGGCCG-3';

S130A, forward primer 5'-CAGGCTGAAGGGGCCCCAGGTGGACCTG-3' and reverse 5'-CAGGTCCACCTGGGGCCCCTTCAGCCTG-3';

T145A forward primer 5'-GAAACCGGCGGCAGGCTAGCATGACAG-3' and reverse 5'-CTGTCATGCTAGCCTGCCGCCGGTTTC-3';

S146A forward primer 5'-CGGCGGCAGACCGCGATGACAGATTTC-3' and reverse 5'-GAAATCTGTCATCGCGGTCTGCCGCCG-3'.

RNAi

NIH3T3 or HeLa cells were seeded at 1 to 1.5 X 10^5 cells/well in 6 well dishes and grown overnight, then transfected with siRNA ON-TARGETplus Smartpools (Dharmacon) against mouse MST2 (STK3; L-040440-00), human MST2 (STK3; J- J 004874-07) or a non-targeting control (NTC; D-001810-01). siRNA was mixed with 200 µl Optimem (Gibco) containing 4 µl Lipofectamine 2000 (Invitrogen) per well and incubated at room temperature for 20 minutes. Cells were grown in 2 ml Optimem and 200 µl of siRNA master mix was added dropwise to each well. After 6 hours DCS was added to a final concentration of 10%. 24 hours after transfection the medium was changed to DMEM containing 10% DCS, supplemented with penicillin and streptomycin and cells were grown for a further 48 hours before treatment and lysis.

RESULTS

Cytoskeleton-associated MST kinases are activated by actin disruption

Although previous studies found that MST1 was predominantly cytoplasmic and could translocate to the nucleus when phosphorylated (36) or caspase cleaved (36), more precise characterization of MST subcellular localization has not been reported. To examine subcellular localization, we expressed FLAG-epitope tagged MST2 in NIH 3T3 cells and found that distribution appeared to be largely diffuse in the cytoplasm and excluded from the nucleus, with a degree of filamentous actin (F-actin) co-localization (Figure 1A). We then used total internal reflection fluorescence (TIRF) microscopy to evaluate MST2 localization adjacent to the cell:substrate interface, which is highly enriched for F-actin structures (21). As compared to the more diffuse cytoplasmic localization observed using standard epifluorescence (Figure 1A, upper), the TIRF image revealed a more distinct pattern that was co-incident with the F-actin staining observed using phalloidin (Figure 1A, lower). There was no appreciable effect of either MST1 or MST2 on F-actin organization (data not shown). In order to examine the distribution of endogenous MST, we first screened commercial MST antibodies, which following siRNA-mediated knockdown of MST1 or MST2 (Figure 1B, left) would display reduced staining by immunofluorescence (IF; Figure 1B, right). The apparently greater MST2 knockdown by IF likely reflects the lower sensitivity of this method. Only one suitable antibody for MST2 was identified in this way, and none for MST1. Endogenous MST2 staining was similar to the transfected FLAG-MST2, with largely cytoplasmic distribution that was excluded from nuclei, and some organization in filamentous structures (Figure 1B). We again used TIRF

microscopy to evaluate MST2 localization adjacent to the F-actin-enriched cell:substrate interface, and found a strikingly similar pattern of distribution of MST2 and F-actin (Figure 1C). These results suggest that a proportion MST2 is associated with the actin cytoskeleton.

We next wished to determine whether disrupting actin structures would affect MST kinase activity. Initially, F-actin disruption was achieved by inhibiting Rho activity with a cell-permeable Tat-fusion form of the *Clostridium botulinum* C3 exoenzyme (45), which inactivates Rho by ADP-ribosylation at Asparagine 41 (3). We took advantage of the ability of immunoprecipitated MST2 to renature following polyacrylamide gel electrophoresis in order to perform in-gel kinase assays using myelin basic protein (MBP) as substrate (17, 52). As shown in Figure 2A, although comparable levels of MST2 were immunoprecipitated, kinase activity was significantly higher following Tat-C3 treatment. To directly disrupt the actin cytoskeleton, cells were treated with two commonly-used F-actin destabilizing drugs: Cytochalasin D (CTD, from *Zygusporium mansonii*) which caps F-actin and stimulates G-actin ATP hydrolysis (47); or Latrunculin B (LTB, from *Latrunculia magnificans*) which binds G-actin monomers and blocks polymerization into filaments (50). As shown in Figure 2B, CTD, LTB and Tat-C3 each significantly disrupted actin structures, although the final cell morphologies were not identical. To decrease experimental variability by reducing the number of sample handling steps and to increase throughput of the kinase assays, we performed in-gel MST kinase assays on whole cell extracts from each condition. Following F-actin disruption, there was increased MBP-activity observed at the identical 57 KDa molecular weight as observed for the immunoprecipitated MST2 (Figure

2C). The identities of the significantly higher molecular weight MBP-phosphorylating proteins are unknown. In each case there was no apparent change in MST1 or MST2 levels (Figure 2C), nor was there appearance of lower molecular weight caspase-cleaved MST forms (data not shown) (27).

Previous studies showed that MST acted as a MAP4K upstream of the JNK SAPK pathway (27). Disruption of actin structures with CTD induced significantly increased phosphorylation of endogenous c-Jun, as determined by quantitative direct scanning of western blots and near-infrared fluorophore conjugated secondary antibodies, which could be significantly reduced by co-administration of the JNK inhibitor SP600125 (Figure 3A) (5). Expression of FLAG-tagged MST1 or MST2 also induced significantly increased levels of c-Jun phosphorylation, which also were significantly reduced by JNK inhibitor SP600125 (Figure 3A). Expression of MST1 or MST2 elevated in-gel MBP kinase activity at the same molecular weight as the endogenous activity, while kinase-dead MST2 was able to inhibit basal MST kinase activity (Figure 3B). JNK1 was immunoprecipitated and assayed for *in vitro* kinase activity using recombinant GST-c-Jun (amino acids 1-79) as substrate, which revealed that JNK1 activity was induced by ectopically expressed MST1 or MST2 (Figure 3C). JNK1 activity was elevated following Tat-C3 treatment, which was reduced by expression of dominant-negative MST2 (Figure 3D). Consistent with this observation, JNK1 activity was elevated following actin disruption by LTB, CTD or Tat-C3 treatment, which again was significantly by dominant-negative MST2 (Figure 3E). Finally, the significant 50% reduction in MST2 expression by siRNA-mediated knockdown was paralleled by a significant 50% reduction in CTD induced c-Jun phosphorylation (Figure 3F). These

results indicate that disruption of the actin cytoskeleton activates MST, which leads to MST-dependent JNK activation and substrate phosphorylation.

Stabilization of p21 by MST and JNK in response to actin disruption

We previously showed that disruption of actin structures and consequent JNK activation stabilized the p21 CDKI using radioactive pulse-chase assays (14). These findings were confirmed in assays using the protein translation inhibitor emetine to block new synthesis (28) and comparing with p21 levels in untreated cells. After 2 hours of emetine treatment, FLAG-tagged p21 protein levels were reduced by ~50% compared to control while ERK2 levels were unchanged, indicating that p21 protein was relatively unstable (Figure 4A and 4B). Inactivation of RhoA by Tat-C3 produced a characteristic shift in mobility due to ADP-ribosylation, and, consistent with previous results (14), stabilized p21 which was reflected by the increased protein level remaining after emetine treatment (Figure 4A and 4B). Actin disruption with CTD or TAT-C3 significantly increased the amount of p21 remaining in the emetine treatment group (Figure 4B). In addition to actin disruption, p21 stabilization could be induced by expression of MST2 or MST1 (Figure 4C). Consistent with our previous finding that the stabilization of p21 following actin disruption was dependent upon the JNK pathway (14), the JNK inhibitor SP600125 (5) significantly reduced MST2-induced p21 stabilization (Figure 4D). The ability of Tat-C3 to stabilize p21 could be reversed by expression of kinase-dead MST2 (Figure 4E) that had also inhibited Tat-C3 induced JNK activation (Figure 3C). Taken together, these data indicate that the stabilization of p21

following actin cytoskeletal disruption results from the MST-mediated activation of the JNK pathway.

The stability of p21 is influenced by phosphorylation (12), although the effects of phosphorylation at specific sites may vary under different conditions and in different cell types. We examined how candidate phosphorylation sites contributed to Tat-C3 induced stabilization by mutating each to non-phosphorylatable alanine residues. Threonine 57 (T57) (35), Serine 98 (S98) (57) and Serine 130 (S130) (35) have each been shown to be phosphorylated by JNK, and in the case of T57 and S130 these phosphorylation were reported to affect p21 stability (35). Phosphorylation on Threonine 145 (T145) and Serine 146 (S146) may also affect p21 protein stability, however, both increased and decreased stabilization have been reported (12). We analyzed the stability of wild-type and point mutants, either with or without Tat-C3 treatment. As before, Tat-C3 treatment resulted in p21 stabilization (Figure 5A, upper left). In contrast, the stability of a T57A mutant was comparable either with or without Tat-C3 (Figure 5A, upper middle), indicating that this site likely contributed to p21 stabilization in response to actin disruption. The S98A (Figure 5A, upper right) and T145A (Figure 5A, lower middle) mutants responded similarly to wild-type p21, indicating that they did not contribute to p21 stabilization. The S130A (Figure 5A, lower left) and S146A (Figure 5A, lower right) were more stable than wild-type p21, suggesting that these sites might contribute to basal protein turnover (48), but were unlikely to contribute to stabilization in response to actin disruption.

We previously found that direct activation of the JNK pathway with the active MAP3K MEKK1 was sufficient to stabilize p21 in radioactive pulse-

chase assays (14). Using the emetine translation inhibition assay, we found that MEKK1 increased p21 stability comparable to Tat-C3 (Figure 5B). In marked contrast, the T57A p21 mutant was no longer stabilized by either Tat-C3 or MEKK1 (Figure 5C). Finally, the ability of MST1 or MST2 to stabilize p21 (Figure 4B) was markedly reduced in the T57A mutant (Figure 5D). These results indicate that the T57 site mediates the JNK-induced stabilization of p21 that results from the activation of this SAPK pathway, either directly or in response to actin disruption via MST kinases.

The ability of JNK to phosphorylate p21 on T57 (35) is associated with a direct interaction between these proteins (49) (55). We wished to determine whether disruption of the actin cytoskeleton would affect the association of JNK with p21. When FLAG-tagged p21 was immunoprecipitated from cells that were untreated or treated with Tat-C3, there was no marked difference in the amount of endogenous JNK1 and JNK2 that was associated (Figure 6A). The ability of recombinant JNK1 to phosphorylate p21 *in vitro* was lost when T57 was mutated to a non-phosphorylatable alanine (Figure 6B), indicating that this site is likely to be the major JNK phosphorylation site. Although consistent with previous studies showing that p21 is a *bona fide* JNK substrate (49), p21 phosphorylation appeared to be less efficient than for recombinant c-Jun (Figure 6B, right panel). These data indicate that the activation of JNK following actin disruption does not affect the association between JNK and p21, but promotes p21 protein stabilization via phosphorylation on T57.

DISCUSSION

As well as providing a structural framework, the actin cytoskeleton also plays integral roles in cell death, survival and proliferation. One way that information about the mechanical stresses that produce strain on the cytoskeleton, or even result in cytoskeletal disintegration, may be transmitted is via the stress-activated protein kinase pathways. The ultimate cellular response to SAPK signalling induced by alterations to the actin cytoskeleton depends on a number of variables including signal intensity and duration, cell type and context. The mechanisms that “sense” the status of actin structures and couple to SAPK pathways have not been characterized in mammalian cells. In this study we report that MST kinases are activated in response to disruption of the actin cytoskeleton, which in turns leads to activation of the JNK SAPK (Figure 7). One effect of MST-JNK activation following actin disruption is the JNK-mediated phosphorylation and consequent stabilization of the CDKI p21. These data reveal the mechanism that links the sensing of cytoskeletal integrity to a key cell cycle regulatory protein.

An intact actin cytoskeleton and normal Rho signalling are required for cell proliferation, whereas Rho inhibition and loss of cytoskeletal integrity are associated with cell-cycle arrest (41) (42) (9) (44) (46) (32). In addition, the arrest of adherent cells placed in suspension has been associated with actin disruption and high p21 levels (25) (58) (10). These findings have prompted the development of inhibitors that are able to block Rho function by targeting critical post-translational modifications as anti-proliferative agents (54). One way this has been achieved is to block the geranylgeranyl transferase I (GGTase I), which catalyzes the attachment of a 20-carbon geranylgeranyl

group to the Cysteine in the carboxyl-terminal CAAX box. GGTase inhibitors efficiently block RhoA modification and consequently lead to p21-mediated cell-cycle arrest (1). An alternative strategy is to inhibit HMG-CoA reductase, which limits geranylgeranyl pyrophosphate production by inhibiting the conversion of HMG-CoA to mevalonate (a five-carbon molecule required for geranylgeranyl pyrophosphate synthesis), resulting in cell-cycle arrest associated with RhoA inactivation and increased p21 levels (20) (19) (18). Following geranylgeranylation, the Rce1 endopeptidase removes the terminal three amino acids from the RhoA CAAX box; and finally the isoprenylated Cysteine is methylated by the isoprenylcysteine carboxyl methyltransferase (ICMT). Genetic inactivation of ICMT inhibited K-Ras and B-Raf-mediated fibroblast transformation by lowering RhoA protein levels and consequently elevating p21 (6). Physiological inactivation of RhoA can be induced in smooth muscle cells by nitric oxide resulting in p21 elevation and inhibition of proliferation (59). These results reinforce the strong requirement for Rho activity to restrict p21 levels in order to permit cell cycle progression and proliferation.

We and others have demonstrated previously that Rho influences p21 levels at least in part by transcriptional mechanisms (1) (42) (38) (30). There are also post-transcriptional mechanisms by which disruption of the actin cytoskeleton increase p21 levels. Agents that act directly on actin filaments, or indirectly via Rho inhibition, induce cell cycle arrest associated with reduced phosphorylation of the retinoblastoma protein by stabilizing p21 protein leading to its accumulation (14) (37). The p21 stabilization results from activation of JNK in response to loss of cytoskeletal integrity (14). The

mechanisms linking the monitoring of cytoskeletal integrity to JNK activation were previously unknown; we now show that the connection between the disruption of the actin cytoskeleton and the consequent JNK activation that leads to p21 stabilization is mediated via MST kinases.

Saccharomyces cerevisiae provide a useful template for studying the connection between the actin cytoskeleton and the regulation of cell cycle progression. Disruption of actin structures activates Ssk2p, which lies upstream of the Hog1 SAPK (7). In turn, Hog1 phosphorylates and stabilizes the CDKI Sic1 with inhibits the CDK Cdc28 (24). In this study, we found that cytoskeletal disruption activates MST, which lies upstream of the JNK SAPK pathway. The CDKI p21 is stabilized by JNK-mediated phosphorylation following actin disruption. Although the individual components are not homologues (*e.g.* MST ≠ Ssk2p, p21 ≠ Sic1), there is a striking similarity in the way that actin disruption activates SAPK signalling leading to phosphorylation and stabilization of a CDKI suggesting the two pathways to be analogous. One possibility is that the larger number of proteins in higher eukaryotes that play similar roles (e.g. multiple MAP4K proteins and CDKIs) has allowed for plasticity in the identities of the individual components that contribute to a functionally analogous mechanism. Alternatively, this may be an example of convergent evolution in which a similar stimulus-response relationship has been selected for, but which use different components to achieve comparable endpoints. The recurrence of cell-cycle checkpoints that monitor the actin cytoskeleton highlights the importance of restricting cell proliferation to the correct environmental context. Loss of these checkpoints may permit anchorage-independent cell proliferation, a hallmark of cancer.

Although MST kinases were identified because of their possible function as MAP4K that regulate SAPK pathways (17), much recent interest has been focused on the *Drosophila* orthologue *hippo*, which is a key regulator of cell growth, proliferation and survival (31). In this signalling pathway *hippo* associates with the *salvador* scaffold protein, and phosphorylates and activates the NDR kinase *warts*, which is homologous to the mammalian Lats tumour suppressors. The activity of *hippo* is influenced by the F-actin binding proteins *merlin* and *expanded*, which can act as cytoskeletal anchors. However, the *hippo*/MST in the *salvador-warts–hippo* signalling network may be completely independent of MST acting upstream of SAPK regulation in response to cytoskeletal disruption. There are examples of kinases acting in distinct signalling pathways by being physically distributed in discrete protein complexes and insulated from potential cross talk. A case in point being GSK3-β, which acts downstream of the insulin receptor to regulate glycogen synthase activity and downstream of Wnt to regulate β-catenin stability (13). Stimulation of cells with insulin does not result in stabilization of β-catenin because signalling is restricted to the pool of GSK3-β not associated with the multi-protein complex that acts in response to Wnt (22). In this manner, the same kinase can be dedicated to distinct signalling pathways and therefore evoking independent downstream responses. That being said, it is interesting that in the context of the *salvador-warts–hippo* signalling complex, *hippo* represses cyclin E transcription while following F-actin disruption MST stabilizes p21 indicating that there is a recurring role of *hippo*/MST as a negative cell cycle regulator independent of its mode of activation.

Active JNK has been found in association with filamentous-actin (F-actin) (29), where it may contribute to regulating actin polymerization and remodelling (4). Although in *Saccharomyces cerevisiae* the MAP3K Ssk2p contributes to actin recovery following osmotic stress, this process is not mediated via the Hog1 SAPK pathway but instead results from the association of Ssk2p with the polarisome complex and the formin protein Bni1p to mediate polarized actin polymerization (8). Using MALDI-TOF mass spectrometry, we identified β-actin as a co-purified protein with MST2, however, purified β-actin did not associate with recombinant MST2 *in vitro* (data not shown), suggesting that any interactions between MST2 and F-actin are likely to be indirect. We did not observe changes in actin organization in cells expressing MST1 or MST2 despite the fact that JNK1 was activated, suggesting that elevated MST-JNK signalling is not sufficient to affect the actin cytoskeleton in basal conditions. However, it remains to be determined whether MST-mediated activation of JNK contributes to actin recovery. A role for MST in a JNK-independent actin recovery complex that employs formin proteins to catalyze actin polymerization is possible but seems unlikely given that the LD domain of Ssk2p that is critical for actin recovery is not present in MST (8).

ACKNOWELDGEMENTS

This research was supported by Cancer Research UK and a grant to M.F.O. from the NIH (CA030721).

REFERENCES

1. **Adnane, J., F. A. Bizouarn, Y. Qian, A. D. Hamilton, and S. M. Sebti.** 1998. p21(WAF1/CIP1) is upregulated by the geranylgeranyltransferase I inhibitor GGTI-298 through a transforming growth factor beta- and Sp1- responsive element: involvement of the small GTPase rhoA. Mol. Cell. Biol. **18:**6962-6970.
2. **Ailenberg, M., and M. Silverman.** 2003. Cytochalasin D disruption of actin filaments in 3T3 cells produces an anti-apoptotic response by activating gelatinase A extracellularly and initiating intracellular survival signals. Biochim. Biophys. Acta **1593:**249-258.
3. **Aktories, K., C. Mohr, and G. Koch.** 1992. Clostridium botulinum C3 ADP-ribosyltransferase. Curr. Top. Microbiol. Immunol. **175:**115-131.
4. **Altan, Z. M., and G. Fenteany.** 2004. c-Jun N-terminal kinase regulates lamellipodial protrusion and cell sheet migration during epithelial wound closure by a gene expression-independent mechanism. Biochem. Biophys. Res. Commun. **322:**56-67.
5. **Bennett, B. L., D. T. Sasaki, B. W. Murray, E. C. O'Leary, S. T. Sakata, W. Xu, J. C. Leisten, A. Motiwala, S. Pierce, Y. Satoh, S. S. Bhagwat, A. M. Manning, and D. W. Anderson.** 2001. SP600125, an anthrapyrazolone inhibitor of Jun N-terminal kinase. Proc. Natl. Acad. Sci. USA **98:**13681-13686.
6. **Bergo, M. O., B. J. Gavino, C. Hong, A. P. Beigneux, M. McMahon, P. J. Casey, and S. G. Young.** 2004. Inactivation of Icmt inhibits

transformation by oncogenic K-Ras and B-Raf. J. Clin. Invest. **113:**539-550.

7. **Bettinger, B. T., and D. C. Amberg.** 2007. The MEK kinases MEKK4/Ssk2p facilitate complexity in the stress signaling responses of diverse systems. J. Cell Biochem. **101:**34-43.

8. **Bettinger, B. T., M. G. Clark, and D. C. Amberg.** 2007. Requirement for the Polarisome and Formin Function in Ssk2p-Mediated Actin Recovery From Osmotic Stress in Saccharomyces cerevisiae. Genetics **175:**1637-1648.

9. **Bohmer, R. M., E. Scharf, and R. K. Assoian.** 1996. Cytoskeletal integrity is required throughout the mitogen stimulation phase of the cell cycle and mediates the anchorage-dependent expression of cyclin D1. Mol. Biol. Cell **7:**101-111.

10. **Bottazzi, M. E., X. Zhu, R. M. Bohmer, and R. K. Assoian.** 1999. Regulation of p21(cip1) expression by growth factors and the extracellular matrix reveals a role for transient ERK activity in G1 phase. J. Cell Biol. **146:**1255-1264.

11. **Cherng, Y. G., H. C. Chang, Y. L. Lin, M. L. Kuo, W. T. Chiu, and R. M. Chen.** 2008. Apoptotic insults to human chondrocytes induced by sodium nitroprusside are involved in sequential events, including cytoskeletal remodeling, phosphorylation of mitogen-activated protein kinase kinase kinase-1/c-Jun N-terminal kinase, and Bax-Mitochondria-Mediated caspase activation. J. Orthop. Res.

12. **Child, E. S., and D. J. Mann.** 2006. The intricacies of p21 phosphorylation: protein/protein interactions, subcellular localization and stability. Cell Cycle **5:**1313-1319.

13. **Cohen, P., and S. Frame.** 2001. The renaissance of GSK3. Nat Rev Mol. Cell. Biol. **2:**769-776.

14. **Coleman, M. L., R. M. Densham, D. R. Croft, and M. F. Olson.** 2006. Stability of p21(Waf1/Cip1) CDK inhibitor protein is responsive to RhoA-mediated regulation of the actin cytoskeleton. Oncogene **25:**2708-2716.

15. **Coleman, M. L., C. J. Marshall, and M. F. Olson.** 2003. Ras promotes p21(Waf1/Cip1) protein stability via a cyclin D1-imposed block in proteasome-mediated degradation. EMBO J, **22:**2036-2046.

16. **Coleman, M. L., E. A. Sahai, M. Yeo, M. Bosch, A. Dewar, and M. F. Olson.** 2001. Membrane blebbing during apoptosis results from caspase-mediated activation of ROCK I. Nat, Cell Biol, **3:**339-345.

17. **Creasy, C. L., and J. Chernoff.** 1995. Cloning and Characterization of a Human Protein Kinase with Homology to Ste20. J. Biol. Chem. **270:**21695-21700.

18. **Danesh, F. R., M. M. Sadeghi, N. Amro, C. Philips, L. Zeng, S. Lin, A. Sahai, and Y. S. Kanwar.** 2002. 3-Hydroxy-3-methylglutaryl CoA reductase inhibitors prevent high glucose-induced proliferation of mesangial cells via modulation of Rho GTPase/ p21 signaling pathway: Implications for diabetic nephropathy. Proc, Natl, Acad, Sci, USA **99:**8301-8305.

19. **Denoyelle, C., P. Albanese, G. Uzan, L. Hong, J. P. Vannier, J. Soria, and C. Soria.** 2003. Molecular mechanism of the anti-cancer activity of cerivastatin, an inhibitor of HMG-CoA reductase, on aggressive human breast cancer cells. Cell Signal **15:**327-338.

20. **Denoyelle, C., M. Vasse, M. Korner, Z. Mishal, F. Ganne, J. P. Vannier, J. Soria, and C. Soria.** 2001. Cerivastatin, an inhibitor of HMG-CoA reductase, inhibits the signaling pathways involved in the invasiveness and metastatic properties of highly invasive breast cancer cell lines: an in vitro study. Carcinogenesis **22:**1139-1148.

21. **Diez, S., G. Gerisch, K. Anderson, A. Muller-Taubenberger, and T. Bretschneider.** 2005. Subsecond reorganization of the actin network in cell motility and chemotaxis. Proc. Natl. Acad. Sci. USA **102:**7601-7606.

22. **Ding, V. W., R. H. Chen, and F. McCormick.** 2000. Differential regulation of glycogen synthase kinase 3beta by insulin and Wnt signaling. J. Biol. Chem. **275:**32475-32481.

23. **Dunn, C., C. Wiltshire, A. MacLaren, and D. A. Gillespie.** 2002. Molecular mechanism and biological functions of c-Jun N-terminal kinase signalling via the c-Jun transcription factor. Cell Signal **14:**585-593.

24. **Escote, X., M. Zapater, J. Clotet, and F. Posas.** 2004. Hog1 mediates cell-cycle arrest in G1 phase by the dual targeting of Sic1. Nat. Cell Biol. **6:**997-1002.

25. **Fang, F., G. Orend, N. Watanabe, T. Hunter, and E. Ruoslahti.** 1996. Dependence of cyclin E-CDK2 kinase activity on cell anchorage. Science **271:**499-502.

26. **Graves, J. D., K. E. Draves, Y. Gotoh, E. G. Krebs, and E. A. Clark.** 2001. Both Phosphorylation and Caspase-mediated Cleavage Contribute to Regulation of the Ste20-like Protein Kinase Mst1 during CD95/Fas-induced Apoptosis. J. Biol. Chem. **276:**14909-14915.

27. **Graves, J. D., Y. Gotoh, K. E. Draves, D. Ambrose, D. K. Han, M. Wright, J. Chernoff, E. A. Clark, and E. G. Krebs.** 1998. Caspase-mediated activation and induction of apoptosis by the mammalian Ste20-like kinase Mst1. EMBO J. **17:**2224-2234.

28. **Grollman, A. P.** 1966. Structural Basis for Inhibition of Protein Synthesis by Emetine and Cycloheximide Based on an Analogy between Ipecac Alkaloids and Glutarimide Antibiotics. Proc. Natl. Acad. Sci. USA **56:**1867-1874.

29. **Hamel, M., D. Kanyi, M. D. Cipolle, and L. Lowe-Krentz.** 2006. Active stress kinases in proliferating endothelial cells associated with cytoskeletal structures. Endothelium **13:**157-170.

30. **Han, S., N. Sidell, and J. Roman.** 2005. Fibronectin stimulates human lung carcinoma cell proliferation by suppressing p21 gene expression via signals involving Erk and Rho kinase. Cancer Lett. **219:**71-81.

31. **Harvey, K., and N. Tapon.** 2007. The Salvador-Warts-Hippo pathway - an emerging tumour-suppressor network. Nat. Rev. Cancer **7:**182-191.

32. **Huang, S., and D. E. Ingber.** 2002. A discrete cell cycle checkpoint in late G(1) that is cytoskeleton- dependent and MAP kinase (Erk)-independent. Exp. Cell Res. **275:**255-264.

33. **Jaffe, A. B., and A. Hall.** 2005. Rho GTPases: biochemistry and biology. Annu. Rev. Cell Dev. Biol. **21:**247-269.

34. **Kaunas, R., S. Usami, and S. Chien.** 2006. Regulation of stretch-induced JNK activation by stress fiber orientation. Cell Signal **18:**1924-1931.

35. **Kim, G. Y., S. E. Mercer, D. Z. Ewton, Z. Yan, K. Jin, and E. Friedman.** 2002. The Stress-activated Protein Kinases p38alpha and JNK1 Stabilize p21Cip1 by Phosphorylation. J. Biol. Chem. **277:**29792-29802.

36. **Lee, K.-K., and S. Yonehara.** 2002. Phosphorylation and Dimerization Regulate Nucleocytoplasmic Shuttling of Mammalian STE20-like Kinase (MST). J. Biol. Chem. **277:**12351-12358.

37. **Lee, Y. J., C. H. Tsai, J. J. Hwang, S. J. Chiu, T. J. Sheu, and P. C. Keng.** 2009. Involvement of a p53-independent and post-transcriptional up-regulation for p21WAF/CIP1 following destabilization of the actin cytoskeleton. Int. J. Oncol. **34:**581-589.

38. **Liberto, M., D. Cobrinik, and A. Minden.** 2002. Rho regulates p21(CIP1), cyclin D1, and checkpoint control in mammary epithelial cells. Oncogene **21:**1590-1599.

39. **Matallanas, D., D. Romano, K. Yee, K. Meissl, L. Kucerova, D. Piazzolla, M. Baccarini, J. K. Vass, W. Kolch, and E. O'Neill.** 2007. RASSF1A elicits apoptosis through an MST2 pathway directing

proapoptotic transcription by the p73 tumor suppressor protein. Mol. Cell **27:**962-975.

40. **O'Neill, E., L. Rushworth, M. Baccarini, and W. Kolch.** 2004. Role of the kinase MST2 in suppression of apoptosis by the proto-oncogene product Raf-1. Science **306:**2267-2270.

41. **Olson, M. F., A. Ashworth, and A. Hall.** 1995. An essential role for Rho, Rac, and Cdc42 GTPases in cell cycle progression through G1. Science **269:**1270-1272.

42. **Olson, M. F., H. F. Paterson, and C. J. Marshall.** 1998. Signals from Ras and Rho GTPases interact to regulate expression of p21Waf1/Cip1. Nature **394:**295-299.

43. **Raman, M., W. Chen, and M. H. Cobb.** 2007. Differential regulation and properties of MAPKs. Oncogene **26:**3100-3112.

44. **Reshetnikova, G., R. Barkan, B. Popov, N. Nikolsky, and L. S. Chang.** 2000. Disruption of the actin cytoskeleton leads to inhibition of mitogen-induced cyclin E expression, Cdk2 phosphorylation, and nuclear accumulation of the retinoblastoma protein-related p107 protein. Exp. Cell Res. **259:**35-53.

45. **Sahai, E., and M. F. Olson.** 2006. Purification of TAT-C3 exoenzyme. Methods Enzymol. **406:**128-140.

46. **Sahai, E., M. F. Olson, and C. J. Marshall.** 2001. Cross-talk between Ras and Rho signalling pathways in transformation favours proliferation and increased motility. EMBO J. **20:**755-766.

47. **Sampath, P., and T. D. Pollard.** 1991. Effects of cytochalasin, phalloidin, and pH on the elongation of actin filaments. Biochemistry **30:**1973-1980.

48. **Scott, M. T., A. Ingram, and K. L. Ball.** 2002. PDK1-dependent activation of atypical PKC leads to degradation of the p21 tumour modifier protein. EMBO J. **21:**6771-6780.

49. **Shim, J., H. Lee, J. Park, H. Kim, and E. J. Choi.** 1996. A non-enzymatic p21 protein inhibitor of stress-activated protein kinases. Nature **381:**804-806.

50. **Spector, I., N. R. Shochet, Y. Kashman, and A. Groweiss.** 1983. Latrunculins: novel marine toxins that disrupt microfilament organization in cultured cells. Science **219:**493-495.

51. **Strange, K., J. Denton, and K. Nehrke.** 2006. Ste20-Type Kinases: Evolutionarily Conserved Regulators of Ion Transport and Cell Volume. Physiology **21:**61-68.

52. **Taylor, L. K., H.-C. R. Wang, and R. L. Erikson.** 1996. Newly identified stress-responsive protein kinases, Krs-1 and Krs-2. Proc. Natl. Acad. Sci. USA **93:**10099-10104.

53. **Ura, S., H. Nishina, Y. Gotoh, and T. Katada.** 2007. Activation of the c-Jun N-Terminal Kinase Pathway by MST1 Is Essential and Sufficient for the Induction of Chromatin Condensation during Apoptosis. Mol. Cell. Biol. **27:**5514-5522.

54. **Walker, K., and M. F. Olson.** 2005. Targeting Ras and Rho GTPases as opportunities for cancer therapeutics. Curr. Opin. Genet. Dev. **15:**62-68.

55. **Yue, X., T. R. Nadja, H. Xiaoman, and C. P. Jill.** 2003. Association of JNK1 with p21waf1 and p53: Modulation of JNK1 activity. Mol. Carcinogenesis **36:**38-44.

56. **Yuzyuk, T., M. Foehr, and D. C. Amberg.** 2002. The MEK kinase Ssk2p promotes actin cytoskeleton recovery after osmotic stress. Mol. Biol. Cell **13:**2869-2880.

57. **Zhan, J., J. B. Easton, S. Huang, A. Mishra, L. Xiao, E. R. Lacy, R. W. Kriwacki, and P. J. Houghton.** 2007. Negative Regulation of ASK1 by p21Cip1 Involves a Small Domain That Includes Serine 98 That Is Phosphorylated by ASK1 In Vivo. Mol. Cell. Biol. **27:**3530-3541.

58. **Zhu, X., M. Ohtsubo, R. M. Bohmer, J. M. Roberts, and R. K. Assoian.** 1996. Adhesion-dependent cell cycle progression linked to the expression of cyclin D1, activation of cyclin E-cdk2, and phosphorylation of the retinoblastoma protein. J. Cell Biol. **133:**391-403.

59. **Zuckerbraun, B. S., D. A. Stoyanovsky, R. Sengupta, R. A. Shapiro, B. A. Ozanich, J. Rao, J. E. Barbato, and E. Tzeng.** 2007. Nitric oxide-induced inhibition of smooth muscle cell proliferation involves S-nitrosation and inactivation of RhoA. Am. J. Physiol. Cell Physiol. **292:**C824-831.

Figures legends

Figure 1. MST2 co-localizes with filamentous actin. (A) NIH 3T3 cells transfected with plasmid encoding FLAG-epitope tagged MST2 were fixed and stained with anti-FLAG antibody and Texas Red phalloidin to visualize filamentous actin structures. Total internal reflection fluorescence (TIRF) microscopy was used to examine MST2 distribution proximal to the cell:substrate interface. While epifluorescence (EPI) microscopy showed that MST2 distribution was a mixture of diffuse and organized, TIRF revealed that MST2 distribution was strikingly similar to the actin filaments observed at the region of the cell that is enriched for these cytoskeletal structures. Scale bar = 10 μm. (B) To validate antibodies for immunofluorescence, MST2 was knocked-down with siRNA in NIH 3T3 cells (left). MST2 levels were comparable in untransfected (Un), mock transfected or non-targeting control (NTC) transfected cells, but were reduced in cells transfected with MST2 siRNA. Untransfected (upper right) and MST2 siRNA transfected (lower right), cells were stained with anti-MST2 antibody and analyzed by immunofluorescence. MST2 knockdown detected by western blotting could also be observed by immunofluorescence with one commercial antibody. Scale bars = 50 μm. (C) NIH 3T3 cells were fixed and stained with anti-MST2 antibody and Texas Red phalloidin to visualize filamentous actin structures. TIRF microscopy was used to examine MST2 distribution proximal to the cell:substrate interface, two examples are shown. As with transfected MST2, TIRF revealed that endogenous MST2 distribution was similar to the actin filaments observed at the region of the cell that is enriched for these cytoskeletal structures. Scale bar = 10 μm.

Figure 2. Actin cytoskeleton disruption activates MST kinases. (A) MST2 immunoprecipitated from NIH 3T3 cells treated with cell-permeable TAT-C3 exoenzyme (0.5 μM) had significantly increased activity relative to untreated control cells using an in-gel kinase assay (*p<0.05 by Student's *t*-test, data are means ± SEM. n=3). Lower band in the kinase assay likely represents immunoprecipitated MST1 due to cross-reactivity of the antibody. Blotting of whole cells extracts (WCE) showed equivalent levels of MST2 and ERK2 in each condition. Treatment with Tat-C3 produced a characteristic change in mobility of a proportion of RhoA. (B) Disruption of the actin cytoskeleton in NIH 3T3 fibroblasts with cytochalasin D (CTD; 200 nM), latrunculin B (LTB; 200 nM) or C3 Tat-C3 (0.5 μM). Cells were fixed and stained with Texas Red phalloidin to visualize filamentous actin structures. (C) Whole cell extracts were separated by SDS-PAGE and in-gel kinases assays carried out with myelin basic protein (MBP) embedded in the gel as kinase substrate. Disruption of the actin cytoskeleton increased MBP phosphorylation at a position coincident with MST1 and MST2 mass. Positions of molecular weight markers as indicated. Quantification of [^{32}P] incorporation revealed that the fold-increase in kinase activity relative to untreated cells was significantly increased in CTD and Tat-C3 treated cells (**p<0.01, *p<0.05 by Student's *t*-test, data are means ± SEM. n=6).

Figure 3. JNK activation by actin disruption via MST. (A) Activation of JNK and sensitivity to JNK inhibitor SP600125 were determined by western blotting for c-Jun phosphorylation (left panel). The ratios of phospho-c-Jun/total c-Jun relative to untreated cells are shown in right panel. Treatment with CTD

significantly induced c-Jun phosphorylation that could be significantly reduced by SP600125, similar to the effects of MST1 or MST2 expression. (*p<0.05 by Student's *t*-test, compared either with untreated cells or with and without SP600125 as indicated, data are means ± SEM. n=3). (B) Expression of FLAG-MST1 or FLAG-MST2 increased MBP kinase activity above basal levels, while a kinase-dead version of MST2 (MST2KD) inhibited basal kinase activity, indicating that it acts in a dominant-negative manner. (C) Expression of FLAG-MST1 or FLAG-MST2 increased endogenous JNK1 kinase activity. JNK1 was immunoprecipitated from transfected cells and assayed for phosphorylation of recombinant c-Jun *in vitro*. (D) Dominant-negative kinase-dead MST2 (MST2KD) inhibited JNK1 kinase activity induced by TatC3 (E) Dominant-negative kinase-dead MST2 (MST2KD) inhibited JNK1 kinase activity induced by actin cytoskeleton disruption (**p<0.01, *p<0.05 by Student's *t*-test, data are means ± SEM. n=13). (F) Knockdown of MST2 by siRNA significantly reduced the CTD induced c-Jun phosphorylation (*p<0.01, by Student's *t*-test, data are means ± SEM. n=3).

Figure 4. Turnover of p21 is inhibited by MST activation of the JNK pathway. (A) Inhibition of protein translation with emetine for 2 h revealed that FLAG-p21 levels decreased while RhoA and ERK2 levels remained constant, indicating that p21 is relatively unstable. Inhibition of RhoA with Tat-C3 maintained p21 levels remaining following emetine treatment, indicating increased protein stability. (B) Disruption of the actin cytoskeleton increased the proportion of p21 remaining following emetine treatment, indicative of increased protein stability. (*p<0.05 by Student's *t*-test, data are means ±

SEM. n=6). (C) Increased levels of p21 following 2 h of emetine treatment in cells expressing FLAG-tagged MST1 or MST2 indicative of increased p21 stability. (D) The increased p21 stability induced by MST2 expression could be reversed by the JNK inhibitor 30 μM SP600125 (SP) (*$p<0.05$ by Student's *t*-test, data are means ± SEM. n=4). (E) Stabilization of p21 induced by Tat-C3 can be reversed by kinase-dead MST2.

Figure 5. Thr57 required for p21 stabilization by actin disruption, MST kinases or JNK. (A) Phosphorylation sites reported to regulate p21 stability were individually mutated to non-phosphorylatable alanine residues. Mutants were expressed and protein levels determined following treatment with or without Tat-C3 and protein synthesis inhibitor emetine as indicated. While Tat-C3 elevated levels of wild-type p21 in emetine treated cells indicating increased protein stability, the non-phosphorylatable T57A mutant was not stabilized in response to Tat-C3. S98A and T145A mutants were stabilized by Tat-C3 compared to untreated cells, while the S130A and S146A mutants appeared to increase basal stability. Therefore, T57 appeared to be the critical site for stabilization in response to Tat-C3. (B) Stabilization of p21 by Tat-C3 or direct activation of the JNK pathway by the MAP3K MEKK1 (C) Stabilization of p21 by Tat-C3 or MEKK1 was reduced in the T57A p21 mutant. (D) The mutant p21 T57A mutant was no longer stabilized by MST1 or MST2.

Figure 6. Association of JNK with p21 and phosphorylation on Thr57. (A) Immunoprecipitated FLAG-tagged p21 co-purifies with endogenous JNK kinases. Treatment with Tat-C3 did not affect the levels of co-purified JNK

protein. (B) The ability of recombinant JNK1 to phosphorylate p21 was greatly reduced by mutation to T57 to alanine.

Figure 7. Model of role played by MST kinases linking the integrity of the actin cytoskeleton via the JNK SAPK pathway to the phosphorylation and stability of p21. (A) Under conditions of actin cytoskeletal integrity, MST kinases have low activity and do not significantly activate the JNK SAPK pathway. As a consequence, p21 is not phosphorylated on Thr57 and is relatively unstable. (B) Following disruption of cytoskeletal integrity, MST become activated, leading to increased JNK SAPK activity and consequently, increased p21 phosphorylation on Thr57 resulting in protein stabilization.

Figure 1

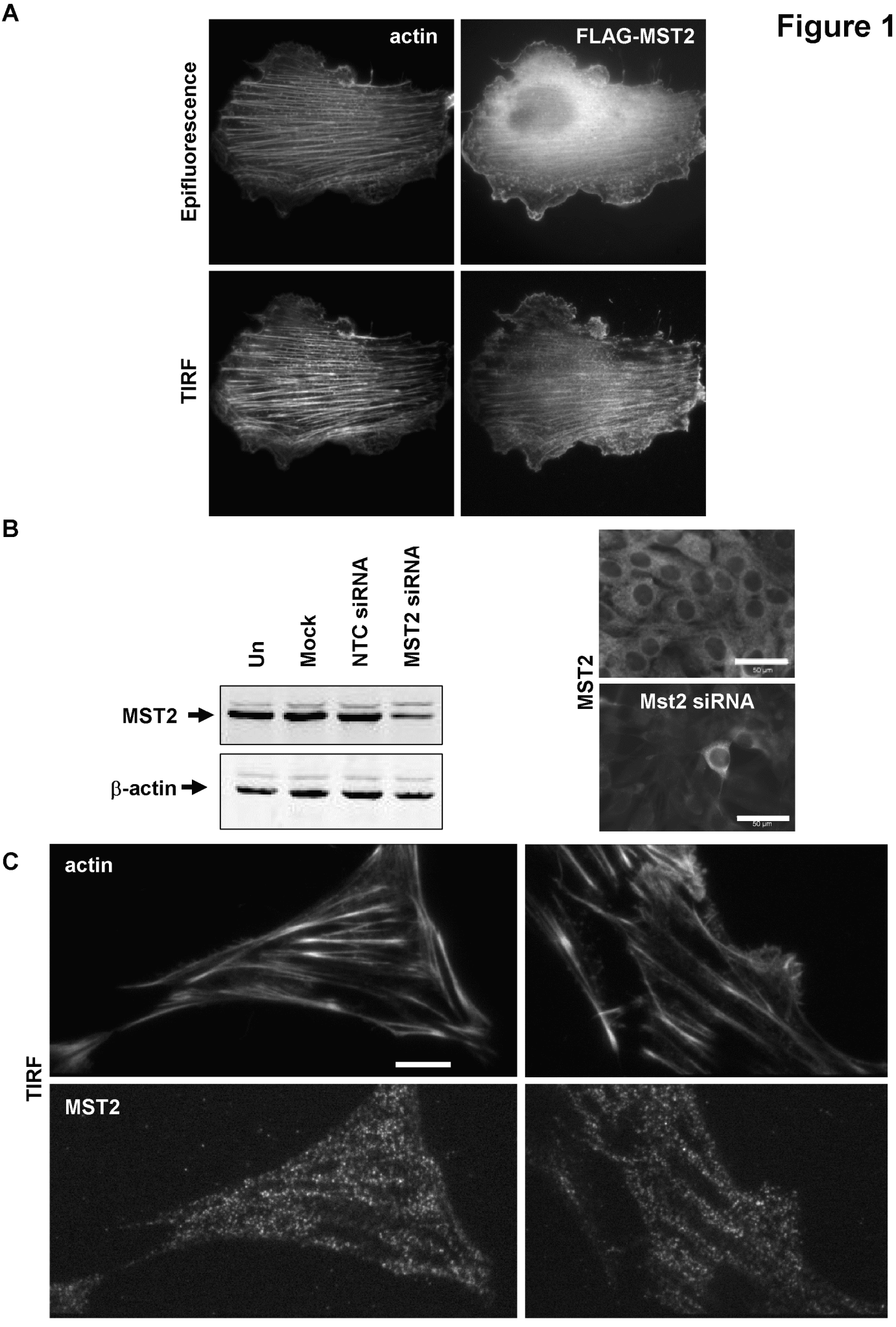
A
actin
FLAG-MST2
Epifluorescence
TIRF
B
Un
Mock
NTC siRNA
MST2 siRNA
MST2
β-actin
MST2
Mst2 siRNA
C
actin
TIRF
MST2

Figure 2

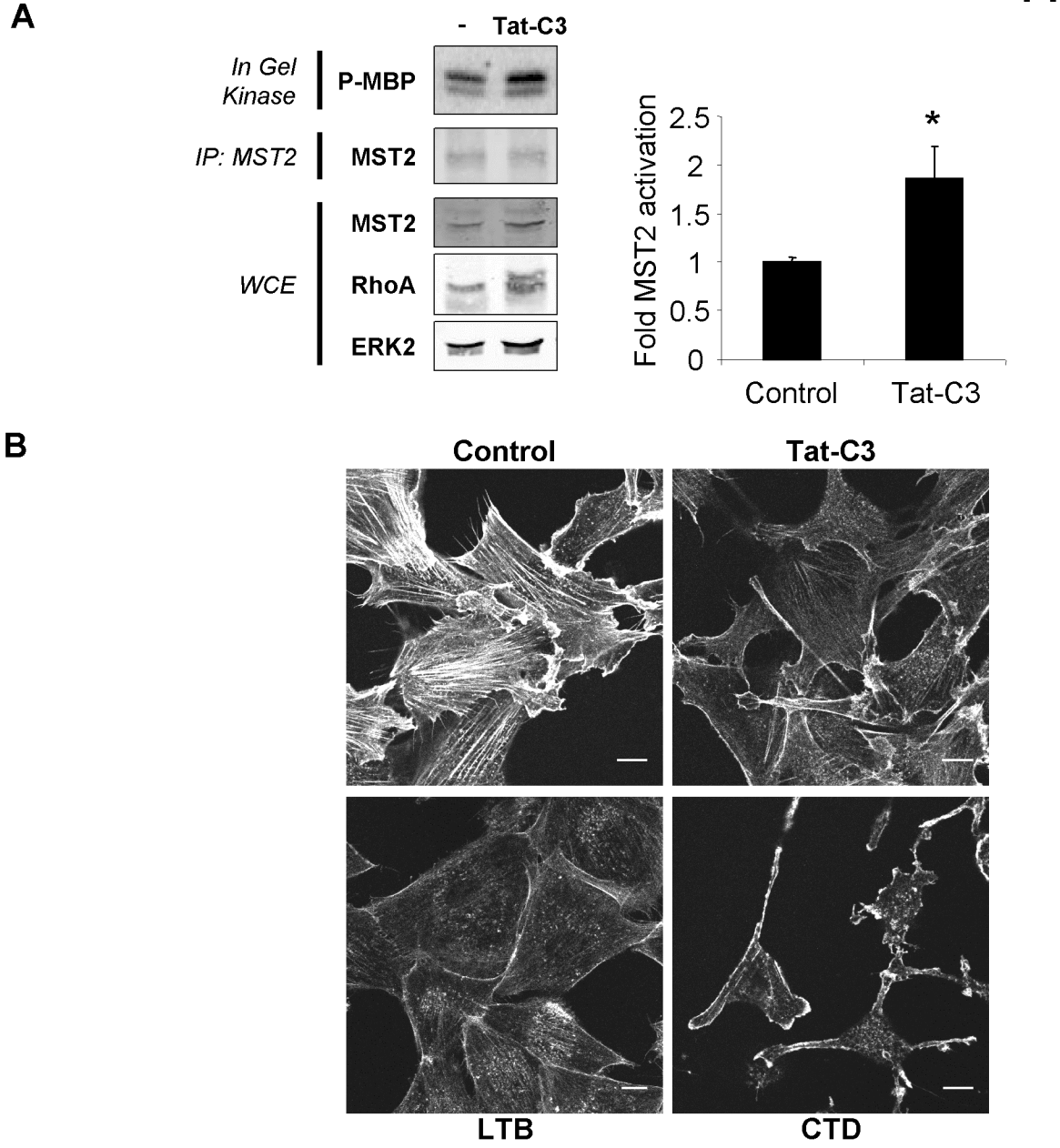
A
- Tat-C3
In Gel Kinase
P-MBP
IP: MST2
MST2
WCE
MST2
RhoA
ERK2
Fold MST2 activation
2.5
2
1.5
1
0.5
0
*
Control
Tat-C3
B
Control
Tat-C3
LTB
CTD
C
-
LTB
CTD
Tat-C3
250
150
100
75
P-MBP
50
In Gel Kinase
WCE
MST1
MST2
β-actin
Fold increase in MST1/2 activity
2.6
2.4
2.2
2
1.8
1.6
1.4
1.2
1
**
*
LTB
CTD
Tat-C3

Figure 3

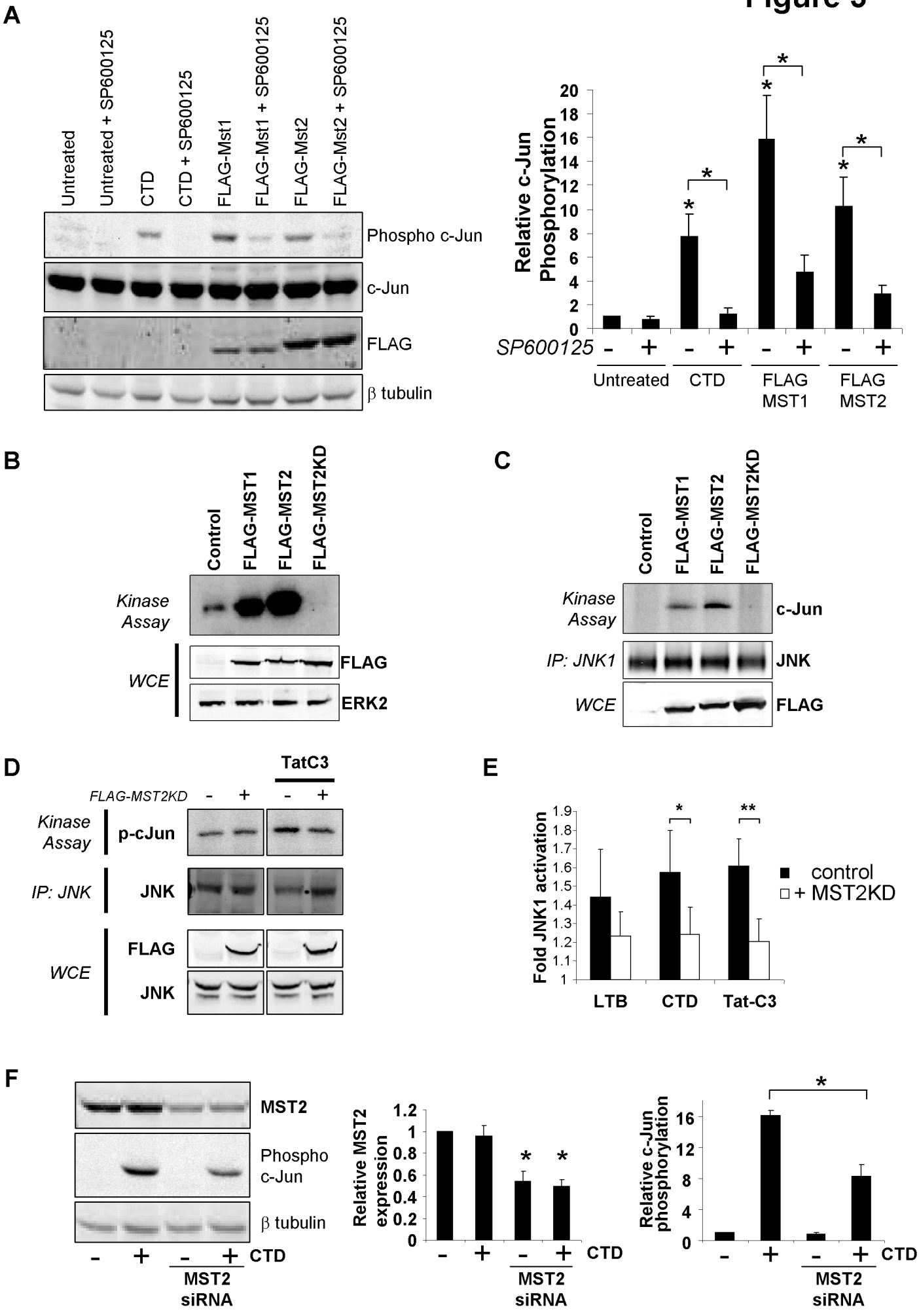
A
Untreated
Untreated + SP600125
CTD
CTD + SP600125
FLAG-Mst1
FLAG-Mst1 + SP600125
FLAG-Mst2
FLAG-Mst2 + SP600125
Phospho c-Jun
c-Jun
FLAG
β tubulin
Relative c-Jun Phosphorylation
SP600125
Untreated
CTD
FLAG MST1
FLAG MST2
B
Control
FLAG-MST1
FLAG-MST2
FLAG-MST2KD
Kinase Assay
WCE
FLAG
ERK2
C
Control
FLAG-MST1
FLAG-MST2
FLAG-MST2KD
Kinase Assay
c-Jun
IP: JNK1
JNK
WCE
FLAG
D
TatC3
FLAG-MST2KD
Kinase Assay
p-cJun
IP: JNK
JNK
WCE
FLAG
JNK
E
Fold JNK1 activation
control
+ MST2KD
LTB
CTD
Tat-C3
F
MST2
Phospho c-Jun
β tubulin
CTD
MST2 siRNA
Relative MST2 expression
Relative c-Jun phosphorylation

Figure 4

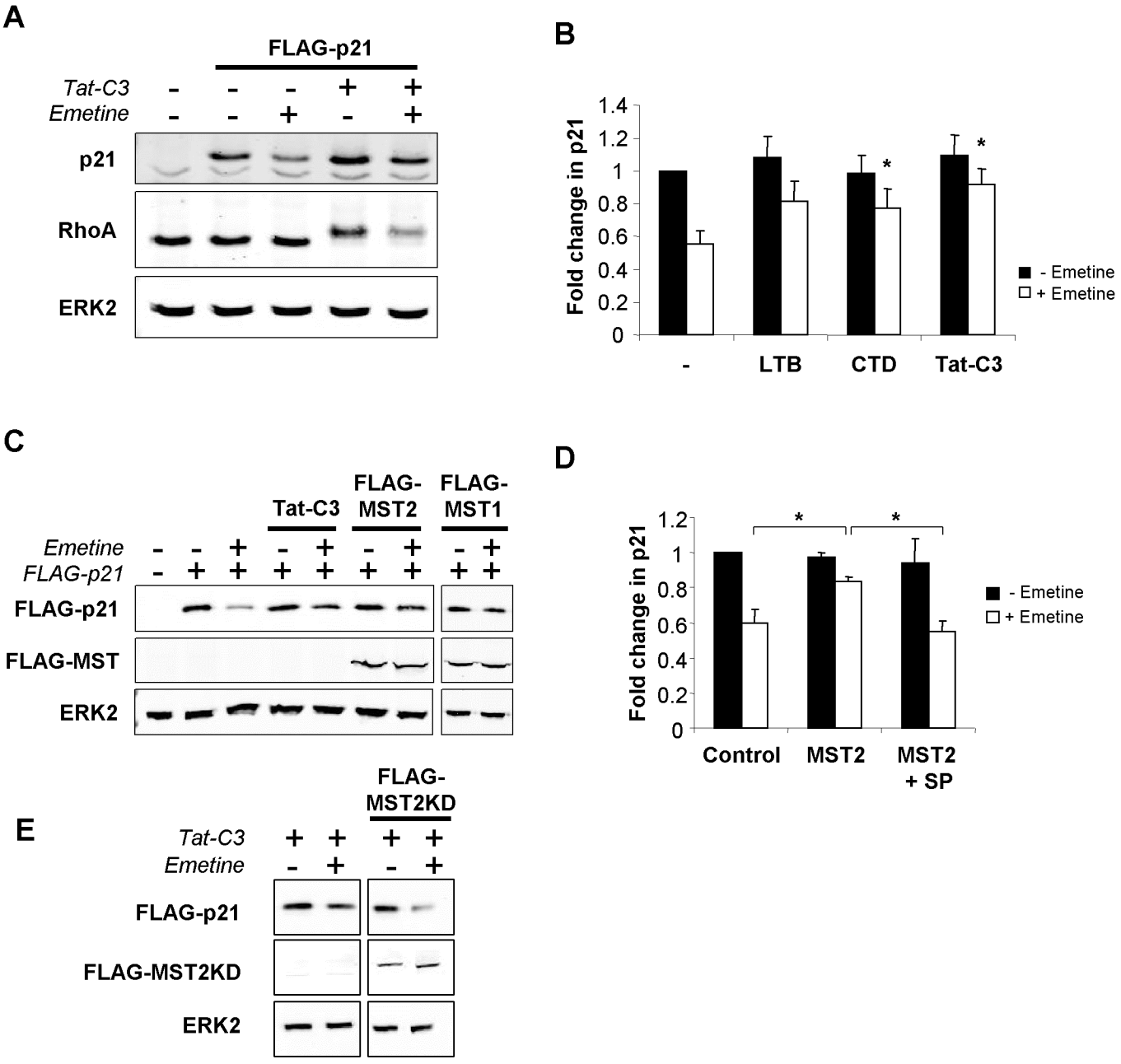
A
FLAG-p21
Tat-C3
Emetine
p21
RhoA
ERK2
B
Fold change in p21
1.4
1.2
1
0.8
0.6
0.4
0.2
0
*
*
- Emetine
+ Emetine
-
LTB
CTD
Tat-C3
C
Tat-C3
FLAG-MST2
FLAG-MST1
Emetine
FLAG-p21
FLAG-p21
FLAG-MST
ERK2
D
Fold change in p21
1.2
1
0.8
0.6
0.4
0.2
0
*
*
- Emetine
+ Emetine
Control
MST2
MST2 + SP
E
FLAG-MST2KD
Tat-C3
Emetine
FLAG-p21
FLAG-MST2KD
ERK2

Figure 5

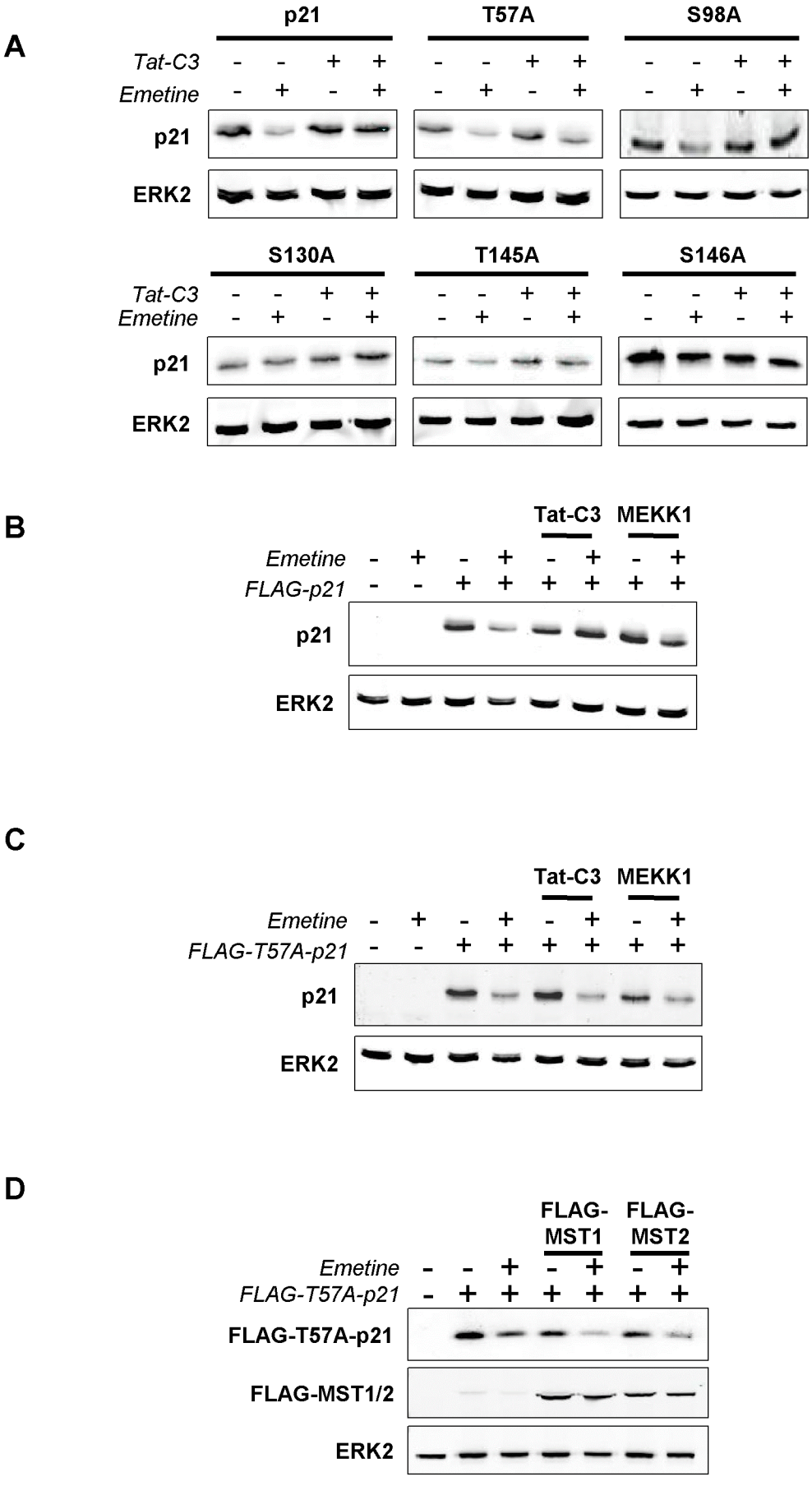
A
p21
T57A
S98A
Tat-C3
Emetine
p21
ERK2
S130A
T145A
S146A
B
Tat-C3
MEKK1
Emetine
FLAG-p21
p21
ERK2
C
Tat-C3
MEKK1
Emetine
FLAG-T57A-p21
p21
ERK2
D
FLAG-MST1
FLAG-MST2
Emetine
FLAG-T57A-p21
FLAG-T57A-p21
FLAG-MST1/2
ERK2

Figure 6

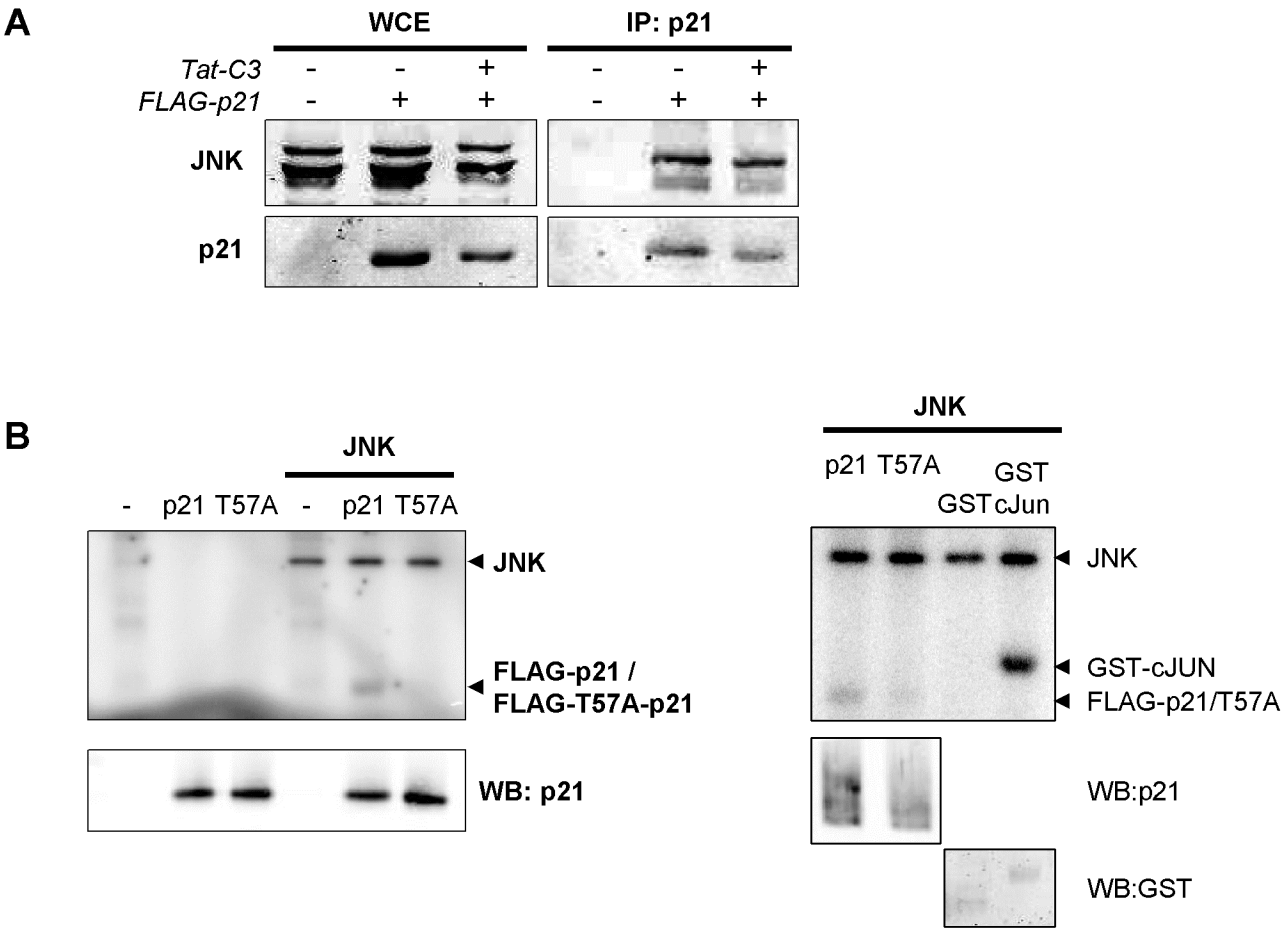
A
WCE
IP: p21
Tat-C3 - - + - - +
FLAG-p21 - + + - + +
JNK
p21
B
JNK
- p21 T57A - p21 T57A
JNK
FLAG-p21 /
FLAG-T57A-p21
WB: p21
JNK
p21 T57A
GST
GST cJun
JNK
GST-cJUN
FLAG-p21/T57A
WB:p21
WB:GST

Figure 7

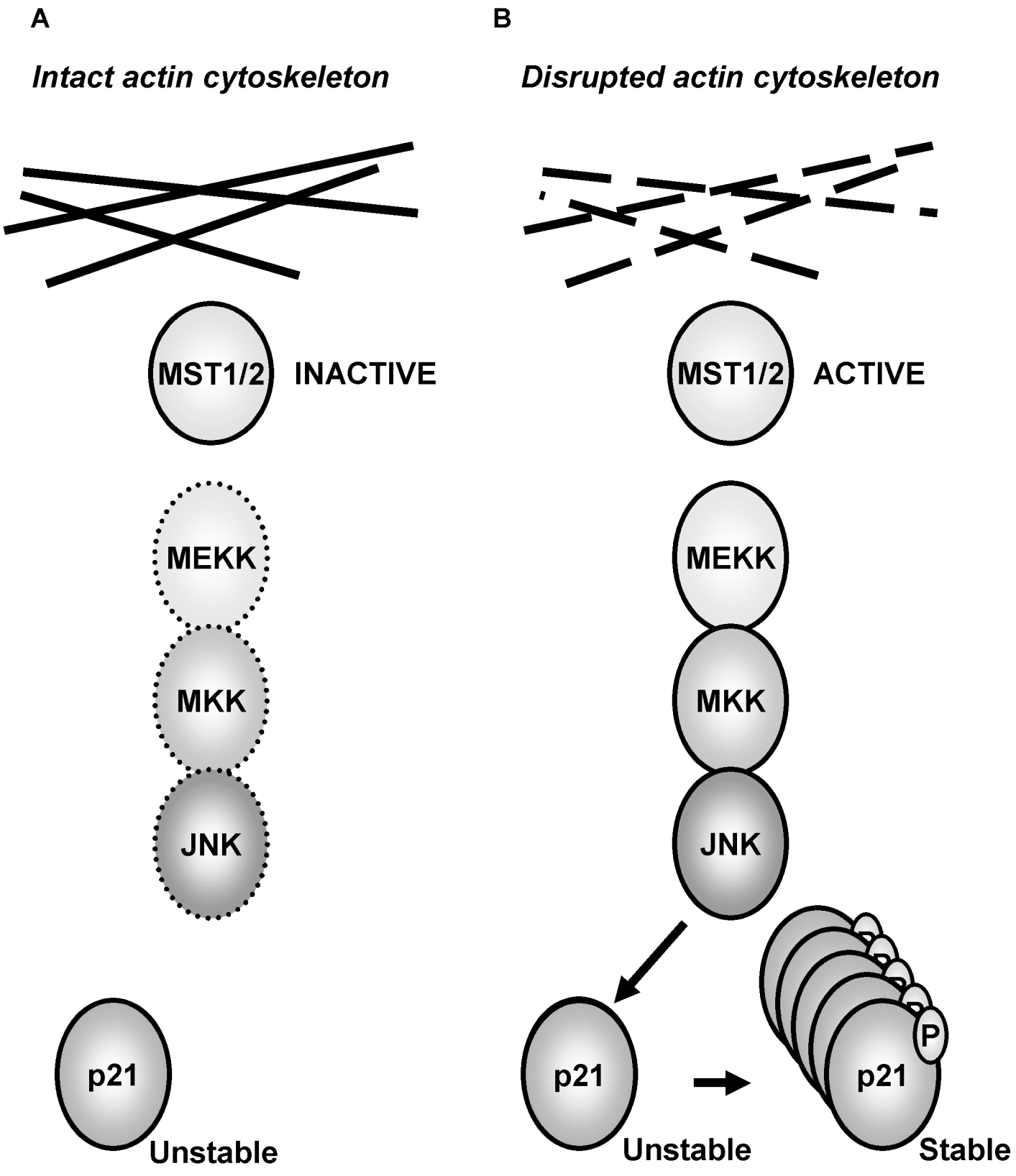
A
Intact actin cytoskeleton
MST1/2
INACTIVE
MEKK
MKK
JNK
p21
Unstable
B
Disrupted actin cytoskeleton
MST1/2
ACTIVE
MEKK
MKK
JNK
p21
Unstable
P
p21
Stable